mater.scichina.com link.springer.com

Sci China Mater 2025, 68(1): 149–155
https://doi.org/10.1007/s40843-024-3134-1

Enhancing negative thermal quenching in green-emitting perovskite microspheres via shallow trap state modulation

Zhenxu Lin[1], Rui Huang[1*], Jie Song[1], Yi Zhang[1], Zewen Lin[1], Hongliang Li[1], Haixia Wu[1], Dejian Hou[1], Yanqing Guo[1], Jing Wang[2*] and Paul K. Chu[3*]

ABSTRACT For luminescent materials, negative thermal quenching (NTQ), characterized by an increase in the luminescent intensity with temperature, has a large potential in lighting and display technologies. However, leveraging NTQ in metal halide perovskites is challenging, and the mechanism is not well understood. Herein, by utilizing low-temperature photoluminescence, persistent luminescence and thermoluminescence, the origins of NTQ in $CsPbBr_3$ microspheres are systematically studied, which pertain to the liberation of carriers from shallow trap states. Experimental and theoretical investigations reveal that the energy of these shallow defect states is approximately 0.135 eV beneath the conduction band. A rapid thermal treatment increases the density of these shallow traps and amplifies the NTQ effect, resulting in an enhancement of room-temperature photoluminescence by more than 60% compared to that at 150 K. The process also reduces the threshold for amplified spontaneous emission to about 45 W/cm^2. Our findings not only provide a deeper understanding of the NTQ phenomenon in $CsPbBr_3$ microspheres but also open new avenues for enhancing the performance of perovskite optoelectronic devices through energy state regulation.

Keywords: negative thermal quenching, photoluminescence, $CsPbBr_3$ microsphere, amplified spontaneous emission, low threshold.

INTRODUCTION

In recent years, metal halide perovskites have emerged as promising materials in optoelectronics due to their high photoluminescence quantum yields (PLQYs), broad visible light absorption, and long carrier lifetimes, which endow them with significant potential in high-performance photoelectronic devices [1–3]. However, compared to traditional fluorescent materials, metal halide perovskites face a severe drop in luminescence intensity with increasing temperature (so-called luminescence thermal quenching, TQ), which significantly limits their widespread application in high-power devices and displays [4–6]. For instance, most metal halide perovskite micro- and nanolasers based on continuous-wave optical pumping can only operate at low temperatures due to TQ, as their high defect state density and strong electron-phonon coupling produce larger non-radiative recombination losses at higher temperatures [6]. Therefore, exploring efficient strategies to reduce non-radiative recombination paths and suppress TQ in metal halide perovskites is crucial for their practical applications in photoelectronic devices.

The most common approach to reduce non-radiative recombination paths is to passivate defects on the surface and in the bulk of the materials, thereby reducing trap state recombination and surface recombination [7–10]. Another effective method involves doping with rare-earth elements to create energy transfer pathways between energy levels to decrease thermal quenching [11–15]. For example, Xia *et al.* [12] have employed heterovalent substitution of Cr^{3+} ions for Mg^{2+} in MgO translucent ceramics to generate a significant number of magnesium vacancies. This alteration activates the phonon-assisted energy transfer between various excited-state levels of different Cr^{3+} ions, yielding an impressive thermal stability of 87.5% at 423 K. To date, some breakthroughs have been made to suppress severe TQ in perovskite nanocrystals (NCs) [16–18]. For instance, Zou *et al.* [16] have reported a strategy using Mn^{2+} substitution to increase the formation energy of $CsPbX_3$ (X = Cl, Br or I) NCs for anti-thermal quenching. Liu *et al.* [18] have demonstrated a fluoride post-synthesis treatment that effectively suppresses emission thermal quenching and enhances the structural thermal stability of $CsPbBr_3$ NCs for temperature-independent light emission up to a temperature of 373 K. Despite these advances, major challenges remain in realizing negative thermal quenching (NTQ) in metal halide perovskites. These challenges are largely attributed to the presence of defects, ion migration, thermal instability, strong exciton-phonon coupling, and complex recombination dynamics. Addressing these issues demands precise control over synthesis and post-treatment techniques, as well as a comprehensive understanding of carrier behavior at different temperatures.

It has been shown that intrinsic defects in perovskites, such as bromine vacancies, iodine vacancies, and lead vacancies, can interact with other chemicals or undergo internal reorganization to form weaker defect states. These defect states typically reside at shallow energy levels [19–21]. Although these shallow defect

[1] School of Materials Science and Engineering, Hanshan Normal University, Chaozhou 521041, China
[2] Ministry of Education Key Laboratory of Bioinorganic and Synthetic Chemistry, State Key Laboratory of Optoelectronic Materials and Technologies, Sun Yat-Sen University, Guangzhou 510275, China
[3] Department of Physics, Department of Materials Science and Engineering, and Department of Biomedical Engineering, City University of Hong Kong, Tat Chee Avenue, Kowloon, Hong Kong, China
* Corresponding authors (rhuang@hstc.edu.cn (Huang R); ceswj@mail.sysu.edu.cn (Wang J); paul.chu@cityu.edu.hk (Chu PK))

states can capture carriers, these carriers can acquire enough energy at room temperature to escape from the shallow defect states back to the conduction or valence band. The presence of shallow defects undoubtedly weakens the electron-phonon coupling effect and reduces the probability of energy loss through phonons. In this respect, shallow defect levels can serve as transit stations for carriers to reduce recombination losses during carrier transport. However, there has been little research on the impact of shallow defects on non-radiative recombination and TQ, but a solid understanding of the photophysical mechanisms is crucial to optimizing the properties of $CsPbX_3$ for optoelectronic applications.

In this work, temperature-dependent PL, persistent luminescence (PersL) and thermoluminescence (TL) measurements were carried out to systematically identify the release process, elucidate the underlying mechanism of carriers moving from shallow trap states, and identify the origins of NTQ in $CsPbBr_3$ microspheres. Shallow defect states are approximately 0.135 eV beneath the conduction band (CB). Moreover, the rapid thermal treatment significantly boosts the shallow trap density, thereby enhancing the NTQ effect. This leads to over a 60% increase in room-temperature PL intensity compared to that at 150 K, while simultaneously reducing the threshold for amplified spontaneous emission (ASE) in $CsPbBr_3$ microspheres.

RESULTS AND DISCUSSION

Optically pumped PL spectroscopy was performed on the $CsPbBr_3$ microspheres. Fig. 1a presents the two-dimensional (2D) pseudo-color maps of the temperature-dependent PL spectra of the microspheres, revealing consistent blue-shifting as the temperature increases from 10 to 300 K in addition to significant broadening of the full-width at half-maximum (FWHM) of the PL peaks. The PL intensity decreases sharply from 10 to 250 K due to thermal quenching. However, an anomalous NTQ effect is observed as the temperature continues to rise from 250 to 300 K, as shown in Fig. 1a, b. This NTQ behavior contrasts with conventional thermal quenching in semiconducting luminescent materials, which is typically attributed to phonon-assisted nonradiative recombination [22,23]. Furthermore, the NTQ effect is more pronounced in the $CsPbBr_3$ microspheres after rapid thermal annealing, as shown in Fig. 1c, d. Specifically, the PL intensity increases by more than 60% when the temperature rises from 150 to 300 K. The PL intensity variation with temperature stems from two competing processes: (1) reduction of the PL intensity due to thermal dissociation of electron-hole pairs and subsequent decrease in exciton population and (2) NTQ effect arising from thermal excitation of electrons from the intermediate states to the initial state of the PL transition. Both thermal quenching and NTQ can be described by a multi-level model [24]:

$$I(T) = I(0)\frac{1+\sum_{q=1}^{w} D_q \exp(-E_q'/k_B T)}{1+\sum_{j=1}^{m} C_j \exp(-E_j/k_B T)}, \quad (1)$$

where T is the temperature, $I(0)$ is the PL intensity at 10 K, k_B is Boltzmann's constant, and C_j and D_q are the respective weight factors. The exponential term in the numerator is associated with the NTQ process, and E_q represents the activation energy for the process that increases the PL intensity with temperature. Conversely, the exponential term in the denominator describes

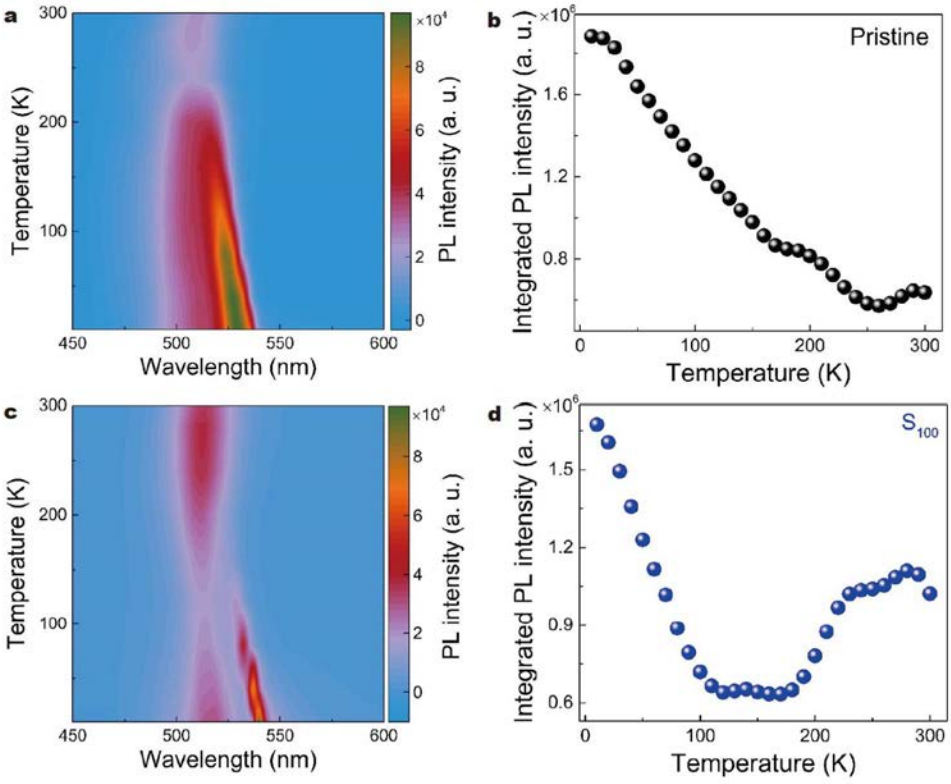

Figure 1 2D pseudo-color maps of the PL spectra as a function of temperatures from 10 to 300 K: (a) pristine $CsPbBr_3$ microspheres and (c) $CsPbBr_3$ microspheres annealed at 205°C with a ramping rate of 100°C/min. Integrated PL intensity as a function of temperature: (b) pristine $CsPbBr_3$ microspheres and (d) $CsPbBr_3$ microspheres annealed at 205°C with a ramping rate of 100°C/min.

the normal thermal quenching process, with E_j representing the activation energy of the process that reduces the PL intensity with temperature. The experimental data can be fitted well by this model, as shown in Fig. 2, showing E_1 = 169 meV, which aligns with the exciton binding energy of $CsPbBr_3$ [25], as well as E_2 = 12 meV, temporarily attributed to the thermal quenching of trapped excitons. Moreover, E_1' = 135 meV suggests the presence of intermediate states approximately 135 meV below CB. These states are often associated with defects, such as vacancies, interstitials, or antisite defects, where multi-carrier trapping-detrapping is expected to contribute to the NTQ of the PL intensity.

To elucidate the role of the intermediate states in NTQ, the PersL characteristics of the $CsPbBr_3$ microspheres were investigated. The samples were irradiated with a 340-nm Xenon lamp for 2 min before the measurement. After turning off the excitation source, the PersL signal remains detectable at a low temperature, as shown in Fig. 3a, indicating the intermediate states are trapping states. It is hypothesized that as the temperature increases, electrons are detrapped thermally from these states into CB, subsequently undergoing radiative recombination with holes to produce the PersL. At 10 K, the PersL spectra exhibit a bimodal structure with peaks at approximately 513 and 540 nm. Fig. 3b illustrates the evolution of the PersL spectra for different decay times at 10 K. Despite the rapid decrease in the PersL intensity, the spectral features are largely unchanged. The 513-nm peak coinciding with the PL peak can be attributed to the recombination of bound excitons [26]. Conversely, the 540-nm peak disappears as the temperature increases to 40 K (Fig. 3a), indicating that this peak results from the radiative recombination of trapped excitons in shallow traps [27]. The 540-nm PersL peak suggests that the trapped excitons are located at energies approximately 12 meV below CB, which aligns with the E_2 value shown in the fitting in Fig. 2. This supports the hypothesis that E_2 represents the activation energy of thermal quenching of trapped excitons in the $CsPbBr_3$ microspheres.

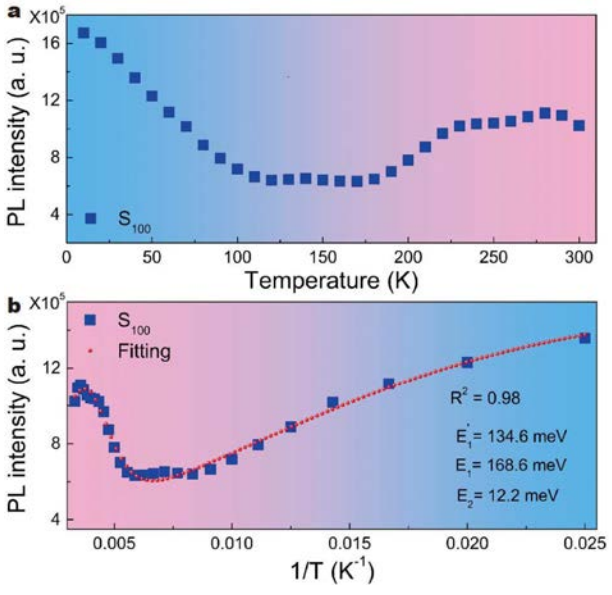

Figure 2 (a) Temperature-dependent PL intensity of $CsPbBr_3$ microspheres annealed at 205°C with a ramping rate of 100°C/min; (b) PL intensity *versus* the inverse of temperature ($1/T$). The fitted curve (red) indicates the contribution of different activation energies to the PL intensities. The fitting parameters are E_1' = 134.6 meV, E_1 = 168.6 meV, and E_2 = 12.2 meV, with an R^2 of 0.98. These energies correspond to different processes in thermal quenching and NTQ.

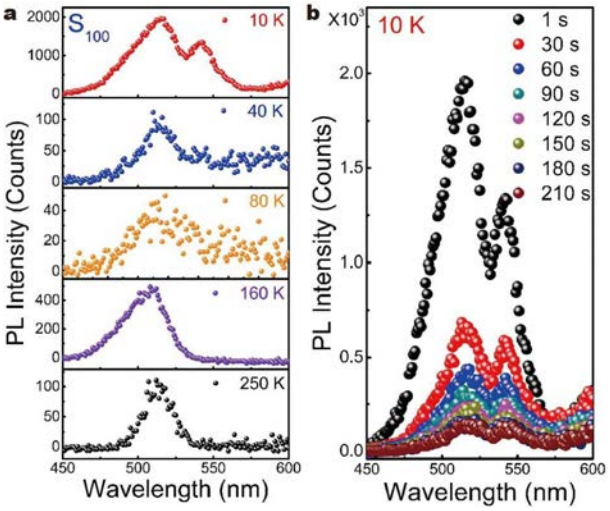

Figure 3 (a) PersL spectra of $CsPbBr_3$ microspheres annealed at 205°C with a ramping rate of 100°C/min acquired at different low temperatures after irradiation by a 340-nm xenon lamp for 2 min. (b) PersL spectra acquired at different decay times at 10 K.

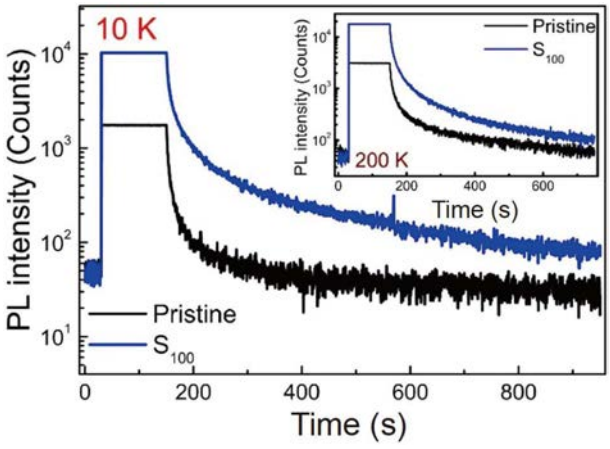

Figure 4 PersL decay curves monitored at 513-nm emission from pristine $CsPbBr_3$ microspheres and $CsPbBr_3$ microspheres annealed at 205°C with a ramping rate of 100°C/min measured at 10 K after irradiation with a 340-nm xenon lamp for 2 min. The inset shows the decay curves at 200 K under the same condition.

Fig. 4 presents the PersL decay curves of the pristine and annealed $CsPbBr_3$ microspheres at 513 nm, and 10 K and 200 K, respectively. Both samples were irradiated with a 340-nm Xenon lamp for 2 min prior to the measurement. The PersL intensity of both samples decreases rapidly in the first 100 s, followed by a slower decay. The initial PersL intensity of the annealed sample is significantly higher, nearly an order of magnitude greater than that of the pristine sample. Even 400 s after turning off the 340-nm excitation source, the PersL intensity of the annealed sample is three times higher than that of the pristine sample. These findings suggest that rapid thermal annealing increases the density of trapping states in the $CsPbBr_3$ microspheres.

To gain further insights into the trapping states, low-tem-

perature TL experiments were conducted. As shown in Fig. 5a, the low-temperature TL monitored at 513 nm of the pristine sample exhibits a broad band from 150 to 290 K, indicating that the trapping states are near the CB edges. Based on the TL band, the trap depths estimated based on the initial rise are about 140 meV, as shown in Fig. S1 (Supplementary information). This is consistent with the fitting parameter E_1' in Fig. 2, further supporting that the intermediate states are the trapping states that contribute to NTQ. In addition to the broad TL band, the low-temperature TL from the annealed samples shows a narrow band with a peak at 25 K, suggesting that these trapping states are very close to the CB edges and have a narrow distribution. Consequently, it is reasonable that the 513-nm PersL cannot be detected at room temperature. Fig. 5a shows that the broad band intensifies significantly after rapid annealing, reflecting more trapping states in the annealed sample. In particular, the sample annealed with a heating rate of 100 K/s exhibits the highest density of states. The inset in Fig. 5 displays the PL spectra of samples treated at different heating rates and measured at room temperature. The sample annealed with a heating rate of 100 K/s shows the highest PL intensity. Additionally, the variation trend of the PL intensity with heating rates at room temperature aligns with that of the TL intensity. This consistency implies that the variations in the PL intensity are closely related to the density of the shallow trapping states. In other words, the higher the density of shallow trap states, the more pronounced the room-temperature PL intensity. According to the multi-level model and TL spectra, it is believed that photoexcited carriers partially relax into shallow trapping states near 135 meV below CB. These carriers later escape to the CB bottom after they have gained

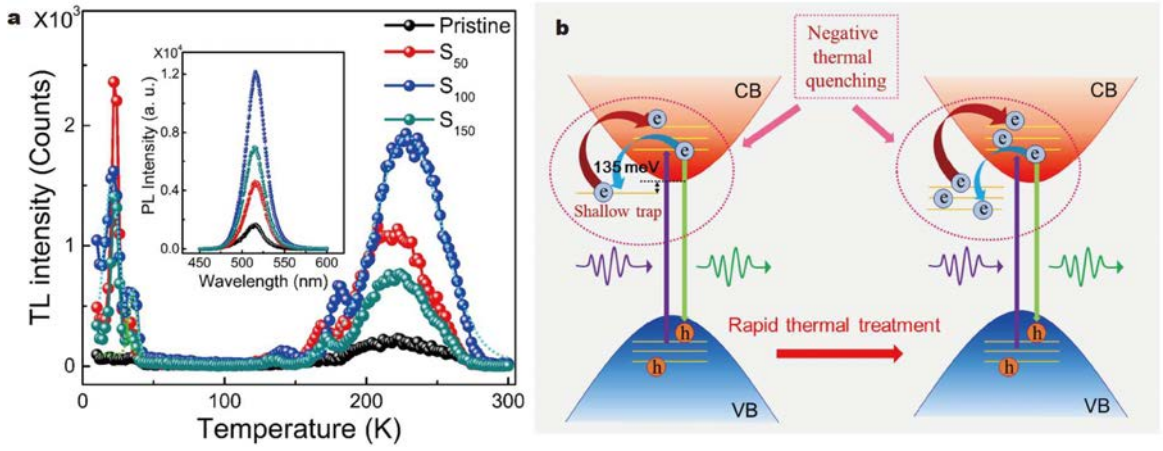

Figure 5 (a) TL curves monitored at 513-nm emission for the pristine $CsPbBr_3$ microspheres and $CsPbBr_3$ microspheres annealed at 205°C with different ramping rates: 50°C/min (red), 100°C/min (blue), and 150°C/min (green) after initial excitation by 340-nm light for 60 s. The inset displays the PL spectra of the corresponding samples measured at room temperature. (b) Schematic energy band diagram illustrating the amplification of NTQ by rapid thermal treatment.

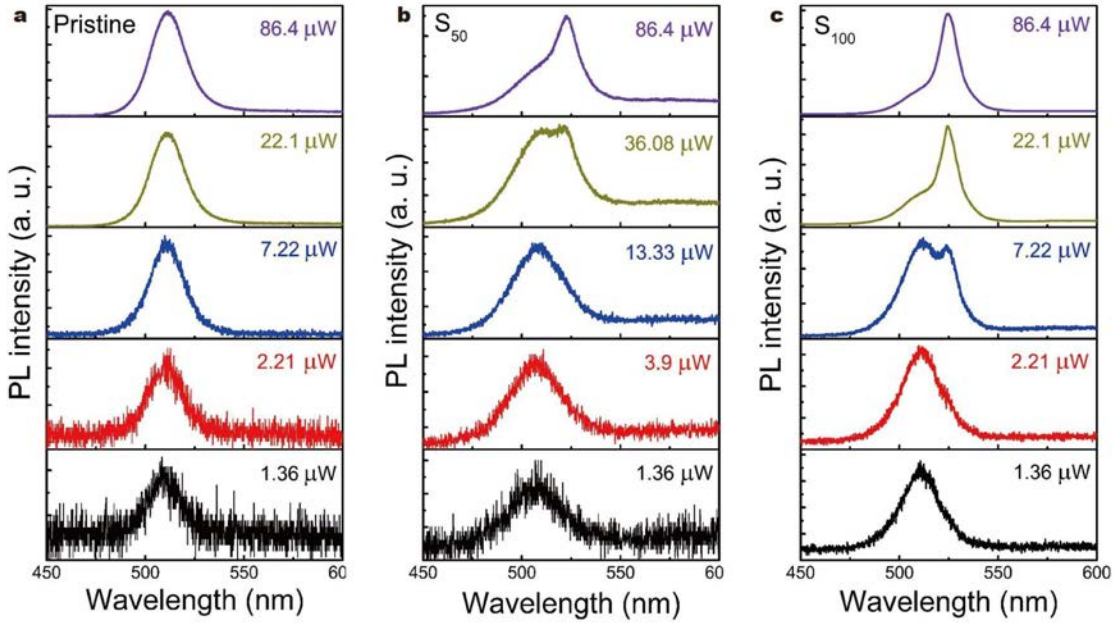

Figure 6 PL spectra for different pump powers for $CsPbBr_3$ microspheres: (a) pristine, (b) annealed at 205°C with a ramping rate of 50°C/min, and (c) annealed at 205°C with a ramping rate of 100°C/min.

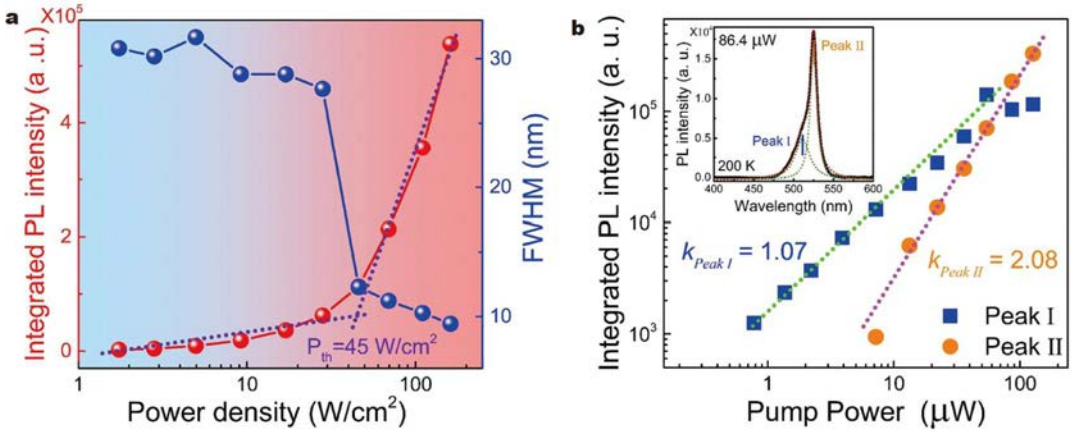

Figure 7 (a) Dependence of the PL intensity and FWHM on the excitation power density observed for the $CsPbBr_3$ microspheres annealed at 205°C with a ramping rate of 100°C. (b) Integrated PL intensity of Peak I (blue squares) and Peak II (orange circles) as a function of pump power for the $CsPbBr_3$ microspheres. The inset shows the separation of Peak I and Peak II in the PL spectrum measured at a pump power of 86.46 μW and a temperature of 200 K. The integrated PL intensity of Peak I follows a linear dependence on the pump power with an exponent $k_{Peak\ I}$ = 1.07, indicating typical exciton emission. In contrast, the integrated PL intensity of Peak II exhibits a superlinear dependence with an exponent $k_{Peak\ II}$ = 2.08 suggestive of biexciton emission.

sufficient energy and undergo radiative band-to-band recombination, as schematically illustrated in Fig. 5b. These shallow trap states are crucial to the emission by transferring some photogenerated carriers, in contrast with the conventional role of traps as centers of non-radiative recombination. Therefore, a larger density of trapping states produces a higher PL intensity at room temperature.

To gain a deeper understanding of the characteristics of trap-modulated PL, we examined the impact of the excitation power on the PL properties of samples with different trap densities at low temperatures (Fig. 6). The pristine sample exhibits no change in the peak position even when the pump power density goes up to 86 W at 200 K (Fig. 6a), because it is dominated by typical exciton emission (Peak I). Conversely, the sample annealed with a heating rate of 100 K/s shows a new emission band (Peak II) with a FWHM of 9 nm and red-shifting by 13 nm compared to Peak I, appearing on the low-energy side as the pump power density goes up to 45 W/cm^2 (Fig. 6c). In Fig. 7a, as the pump power density increases to 45 W/cm^2, a noticeable spectral narrowing (FWHM reduced to approximately 9–11 nm) is observed, along with a superlinear rise in PL intensity. These features clearly signify the transition from SE to ASE [28]. Fig. 7b illustrates the integrated PL intensity of Peak I and Peak II as a function of pump power density, respectively. The linear and quadratic dependencies of the PL intensities of these two bands on the pump power intensity confirm exciton emission and biexciton emission, respectively [29,30]. Therefore, it is considered that ASE originates from bi-excitonic recombination [31]. Fig. 6b shows that a large pump power density of more than 36 W is required to obtain the ASE signal from the sample annealed with a heating rate of 50 K/s. By correlating these findings with the trapping state density of the samples (Fig. 4), it is evident that a higher trap state density reduces the ASE threshold and achieves ASE. At elevated temperatures (above 250 K), no ASE is observed, likely because the enhanced thermal excitation effects at elevated temperatures make it difficult for biexcitons to remain stable [32]. Furthermore, the interaction between phonons and excitons intensifies at higher temperatures, resulting in increased exciton scattering and hindering the formation of stable biexcitons [33]. Nevertheless, we observed a gradual increase in PL with rising temperature (see Fig. 1d), suggesting that the enhancement in PL at higher temperatures originates from single excitons rather than biexcitons. The PL lifetime increases with temperature (above 250 K) (Fig. 8), suggesting that the emission arises from electrons transitioning from deeper trapping states, which require more thermal energy to return to CB. However, higher thermal excitation energy inevitably enhances thermal effects, complicates the stability of biexcitons, and impedes ASE. In contrast, electrons in shallow trapping states can acquire sufficient energy to transition to CB at lower temperatures. The smaller thermal excitation energy required for these transitions mitigates the thermal excitation effects and facilitates biexciton formation to enable ASE. All in all, these shallow trapping states play crucial roles in not only amplifying the NTQ effect, but reducing the threshold of ASE as well.

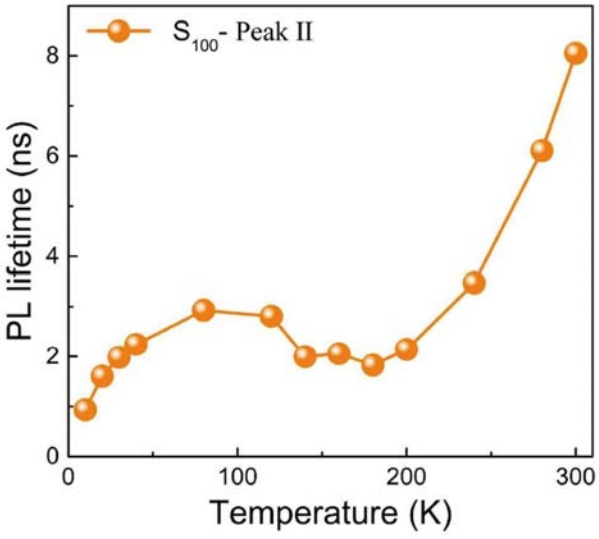

Figure 8 Temperature-dependent PL lifetime of Peak II from $CsPbBr_3$ microspheres annealed at 205°C with a ramping rate of 100°C/min.

CONCLUSIONS

The mechanisms of NTQ in $CsPbBr_3$ microspheres are explored, and the effect is amplified by reducing the threshold of amplified spontaneous emission. By performing low-temperature PL and TL, it is determined that NTQ in the microspheres is driven by the release of carriers from shallow trapping states approximately 0.135 eV below CB. The rapid thermal treatment significantly increases the density of the shallow traps, resulting in a substantial enhancement of the PL intensity by over 60% at room temperature and reducing the threshold of amplified spontaneous emission to about 45 W/cm^2. Our findings reveal that shallow trapping states play a critical role in modulating the luminescence properties of $CsPbBr_3$ microspheres, in contrast to their conventional role as centers for non-radiative recombination. These new results not only provide a deeper understanding of NTQ, but also reveal new avenues to develop low-threshold metal halide perovskite micro-lasers for the advancement of perovskite materials in optoelectronics.

Received 22 August 2024; accepted 23 September 2024; published online 6 November 2024

1 Elkhouly K, Goldberg I, Zhang X, *et al.* Electrically assisted amplified spontaneous emission in perovskite light-emitting diodes. Nat Photon, 2024, 18: 132–138
2 Bai W, Xuan T, Zhao H, *et al.* Perovskite light-emitting diodes with an external quantum efficiency exceeding 30%. Adv Mater, 2023, 35: 2302283
3 Lin Z, Huang R, Zhang W, *et al.* Highly luminescent and stable Si-based $CsPbBr_3$ quantum dot thin films prepared by glow discharge plasma with real-time and *in situ* diagnosis. Adv Funct Mater, 2018, 28: 1805214
4 Du W, Zhang S, Wu Z, *et al.* Unveiling lasing mechanism in $CsPbBr_3$ microsphere cavities. Nanoscale, 2019, 11: 3145–3153
5 Zhang XY, Pang GT, Xing GC, *et al.* Temperature dependent optical characteristics of all-inorganic $CsPbBr_3$ nanocrystals film. Mater Today Phys, 2020, 15: 100259
6 Zhao F, Ren A, Li P, *et al.* Toward continuous-wave pumped metal halide perovskite lasers: strategies and challenges. ACS Nano, 2022, 16: 7116–7143
7 Zhang J, Xing X, Qian D, *et al.* Sulfonic zwitterion for passivating deep and shallow level defects in perovskite light-emitting diodes. Adv Funct Mater, 2022, 32: 2111578
8 Li X, Cai W, Guan H, *et al.* Highly stable $CsPbBr_3$ quantum dots by silica-coating and ligand modification for white light-emitting diodes and visible light communication. Chem Eng J, 2021, 419: 129551
9 Zhang D, Fu Y, Zhan H, *et al.* Suppressing thermal quenching via defect passivation for efficient quasi-2D perovskite light-emitting diodes. Light Sci Appl, 2022, 11: 69
10 Shen X, Kang K, Yu Z, *et al.* Passivation strategies for mitigating defect challenges in halide perovskite light-emitting diodes. Joule, 2023, 7: 272–308
11 Wei Y, Yang H, Gao Z, *et al.* Strategies for designing antithermal-quenching red phosphors. Adv Sci, 2020, 7: 1903060
12 Liu G, Chen W, Xiong Z, *et al.* Laser-driven broadband near-infrared light source with watt-level output. Nat Photon, 2024, 18: 562–568
13 Liu Q, Chen Z, Chen X, *et al.* Defect modulation and luminescence improvement of Mn^{4+}-activated La(Mg, Nb)O_3 phosphor with improved stability for plant cultivation. J Mater Chem C, 2022, 10: 3472–3479
14 Miao S, Liang Y, Zhang Y, *et al.* Spectrally tunable and thermally stable near-infrared luminescence in $Na_3Sc_2(PO_4)_3:Cr^{3+}$ phosphors by Ga^{3+} co-doping for light-emitting diodes. J Mater Chem C, 2022, 10: 994–1002
15 Dang P, Wang W, Lian H, *et al.* How to obtain anti-thermal-quenching inorganic luminescent materials for light-emitting diode applications. Adv Opt Mater, 2022, 10: 2102287
16 Zou S, Liu Y, Li J, *et al.* Stabilizing cesium lead halide perovskite lattice through Mn(II) substitution for air-stable light-emitting diodes. J Am Chem Soc, 2017, 139: 11443–11450
17 Han JH, Viswanath NSM, Park YM, *et al.* Zero-thermal-quenching layered metal halide perovskite. Chem Mater, 2022, 34: 5690–5697
18 Liu M, Wan Q, Wang H, *et al.* Suppression of temperature quenching in perovskite nanocrystals for efficient and thermally stable light-emitting diodes. Nat Photonics, 2021, 15: 379–385
19 Yu H, Zhang T, Zhang Z, *et al.* High defect tolerance β-$CsSnI_3$ perovskite light-emitting diodes. Mater Horiz, 2024, 11: 4730–4736
20 Kim GW, Petrozza A. Defect tolerance and intolerance in metal-halide perovskites. Adv Energy Mater, 2020, 10: 2001959
21 Kang J, Wang LW. High defect tolerance in lead halide perovskite $CsPbBr_3$. J Phys Chem Lett, 2017, 8: 489–493
22 Callsen G, Wagner MR, Kure T, *et al.* Optical signature of Mg-doped GaN: Transfer processes. Phys Rev B, 2012, 86: 075207
23 Reshchikov MA, Kvasov AA, Bishop MF, *et al.* Tunable and abrupt thermal quenching of photoluminescence in high-resistivity Zn-doped GaN. Phys Rev B, 2011, 84: 075212
24 Prashanthi K, Antić Ž, Thakur G, *et al.* Surface state-induced anomalous negative thermal quenching of multiferroic $BiFeO_3$ nanowires. Physica Rapid Res Ltrs, 2018, 12: 1700352
25 Yuan S, Wang ZK, Zhuo MP, *et al.* Self-assembled high quality $CsPbBr_3$ quantum dot films toward highly efficient light-emitting diodes. ACS Nano, 2018, 12: 9541–9548
26 Yang H, Zhang Y, Pan J, *et al.* Room-temperature engineering of all-inorganic perovskite nanocrsytals with different dimensionalities. Chem Mater, 2017, 29: 8978–8982
27 Lao X, Yang Z, Su Z, *et al.* Luminescence and thermal behaviors of free and trapped excitons in cesium lead halide perovskite nanosheets. Nanoscale, 2018, 10: 9949–9956
28 Wang Y, Li X, Song J, *et al.* All-inorganic colloidal perovskite quantum dots: a new class of lasing materials with favorable characteristics. Adv Mater, 2015, 27: 7101–7108
29 Xu Y, Chen Q, Zhang C, *et al.* Two-photon-pumped perovskite semiconductor nanocrystal lasers. J Am Chem Soc, 2016, 138: 3761–3768
30 Grim JQ, Christodoulou S, di Stasio F, *et al.* Continuous-wave biexciton lasing at room temperature using solution-processed quantum wells. Nat Nanotech, 2014, 9: 891–895
31 Zhao W, Qin Z, Zhang C, *et al.* Optical gain from biexcitons in $CsPbBr_3$ nanocrystals revealed by two-dimensional electronic spectroscopy. J Phys Chem Lett, 2019, 10: 1251–1258
32 Lin Y, Zheng X, Shangguan Z, *et al.* All-inorganic encapsulation for remarkably stable cesium lead halide perovskite nanocrystals: Toward full-color display applications. J Mater Chem C, 2021, 9: 12303–12313
33 Thouin F, Srimath Kandada AR, Valverde-Chávez DA, *et al.* Electron–phonon couplings inherent in polarons drive exciton dynamics in two-dimensional metal-halide perovskites. Chem Mater, 2019, 31: 7085–7091

Acknowledgement This work was supported by Guangdong Basic and Applied Basic Research Foundation, Research Projects of Department of Education of Guangdong Province (2021ZDJS039 and 2024ZDZX1026), and the City University of Hong Kong Donation Research Grants (9220061 and DON-RMG 9229021).

Funding note Open Access funding provided by City University of Hong Kong.

Author contributions Lin Z, Huang R, Song J and Wu H designed and performed the experiments; Lin Z wrote the paper with support from Huang R, Wang J and Chu PK. All authors contributed to the general discussion.

Conflict of interest The authors declare that they have no conflict of interest.

Supplementary information Supplementary materials are available in the online version of the paper.

Zhenxu Lin received his BS in physics from Hanshan Normal University and his PhD in optics from the South China Normal University. His research focuses on the design and synthesis of optoelectronic materials and devices based on silicon and pervoskite materials.

Rui Huang received his BS in physics from Hanshan Normal University and his PhD in microelectronics from Nanjing University. He was a visiting researcher at Hong Kong University of Science and Technology and the University of Cambridge. Currently, he is a professor at Hanshan Normal University, focusing on the design and synthesis of optoelectronic materials and devices, with a particular emphasis on light-emitting materials and devices.

Jing Wang received his BS degree in materials chemistry from the Northwest University and PhD in chemistry from Changchun Institute of Applied Chemistry, Chinese Academy of Sciences from 1999 to 2004. Now he is a professor at Sun Yat-sen University. His research focuses on rare earth phosphors, glass/ceramic materials for solid-state lighting and display, and rare earth perovskite nanocrystals for ultra-high definition display.

Paul K. Chu received his PhD from Cornell University and is Chair Professor of materials engineering at City University of Hong Kong. His research focuses on plasma and materials science and engineering.

浅陷阱态调控增强绿色发光钙钛矿微球的负热猝灭效应

林圳旭[1], 黄锐[1*], 宋捷[1], 张毅[1], 林泽文[1], 李洪亮[1], 吴海霞[1], 侯得健[1], 郭艳青[1], 王静[2*], 朱剑豪[3*]

摘要 发光材料中的负热猝灭(NTQ)现象, 表现为随温度升高发光强度增加, 在照明和显示技术中具有广泛应用前景. 然而, 在金属卤化物钙钛矿中实现NTQ具有一定挑战性, 其机制尚不完全清楚. 本研究通过低温光致发光、长余辉和热释光谱技术, 系统研究了$CsPbBr_3$微球中NTQ现象的起源. 结果表明, NTQ现象与浅陷阱态中载流子的释放密切相关. 实验与理论分析揭示, 这些浅缺陷态的能级位于导带下方约0.135 eV处. 快速热处理可显著增加浅陷阱的密度, 从而增强NTQ效应, 使室温下的光致发光强度较150 K时提高了60%以上. 同时, 该处理将受激自发辐射的阈值降低至约45 W/cm^2. 本研究不仅加深了对$CsPbBr_3$微球中NTQ机制的理解, 也为通过能态调控提升钙钛矿光电子器件性能开辟了新途径.

Enhancing Negative Thermal Quenching in Green-Emitting Perovskite Microspheres via Shallow Trap State Modulation

Zhenxu Lin[1], Rui Huang,[1]* Jie Song[1], Yi Zhang[1], Zewen Lin[1], Hongliang Li[1], Haixia Wu[1], Dejian Hou[1], Yanqing Guo[1], Jing Wang,[2]* and Paul K. Chu[3]*

[1] School of Materials Science and Engineering, Hanshan Normal University, Chaozhou, 521041, China

[2] Ministry of Education Key Laboratory of Bioinorganic and Synthetic Chemistry, State Key Laboratory of Optoelectronic Materials and Technologies,Sun Yat-Sen University,Guangzhou, 510275, China

[3] Department of Physics, Department of Materials Science and Engineering, and Department of Biomedical Engineering,City University of Hong Kong, Tat Chee Avenue, Kowloon, Hong Kong, China

* Corresponding author

rhuang@hstc.edu.cn (R. Huang), ceswj@mail.sysu.edu.cn (J. Wang), paul.chu@cityu.edu.hk (P. K. Chu)

Experimental Section/Methods

Fabrication of $CsPbBr_3$ microspheres

The $CsPbBr_3$ microspheres were fabricated on SiO_2/Si substrates by chemical vapor deposition (CVD) under normal pressure with cesium bromide (1 mmol, CsBr, Aladdin, 99.9%) and lead bromide (2 mmol, $PbBr_2$, Macklin, 99.9%) as precursors. The precursor mixture was placed at the center of a quartz furnace at 630°C, while the SiO_2/Si substrates were positioned downstream from the furnace center. The tube furnace was evacuated to a pressure of 5 Pa, and argon was introduced at a flow rate of 100 sccm. The temperature of the tube furnace was then increased to 630 °C within 30 minutes and maintained for 30 minutes to form the $CsPbBr_3$ microspheres before natural cooling to room temperature. Throughout the growth, the argon flow rate was kept at 100 sccm. More details about the procedures can be found in Ref. [1]. The pristine sample was annealed at 205°C at different heating rates in a nitrogen atmosphere for 5 minutes, while the other samples annealed at heating rates of 50 ℃/min, 100 ℃/min, and 150 ℃/min were designated S_{50}, S_{100}, and S_{150}, respectively.

Characterization of $CsPbBr_3$ microspheres

The morphology and composition of the $CsPbBr_3$ microspheres were characterized by scanning electron microscopy (SEM) (Hitachi SU5000), and energy-dispersive X-ray spectroscopy (EDS) (Bruker EDS QUANTAX), as shown in Figure S2 (Supporting information). The PL spectra were obtained on a Raman spectrometer (Horiba LabRAM HR Evolution) equipped with a 325 nm He-Cd laser (Kimmon), with the

samples mounted on a thermal stage (Linkam FTIR-600). The temperature-dependent PL spectra, TL curves, PersL decay curves, and time-resolved PL spectra were acquired on the PL spectrometer (FLS1000, Edinburgh Instrument) equipped with a 372 nm picosecond laser pulses of 20 MHz at a low pump power of 10 μW with the samples mounted on an optical cryostat (Oxford OptistatDry BLV).

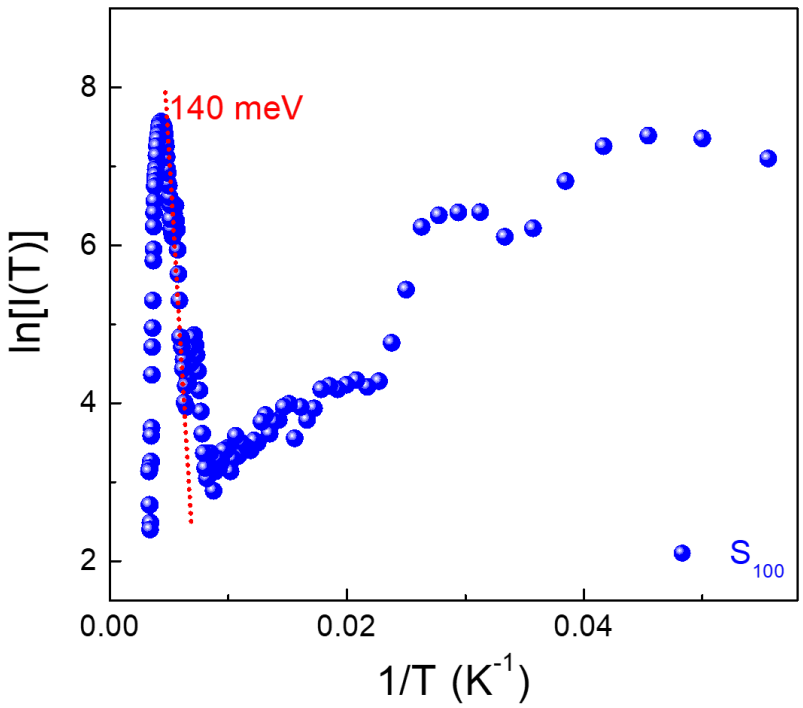

Figure S1 The initial rise method was used to estimate the depths of electron traps. The experimental data was fitted by the equation $I(T) = C \times \exp(\frac{-E}{k_b T})$, where I is the TL intensity, T is the temperature, k_b is Boltzmann constant, and C is the fitting constant [2]. By plotting ln(TL intensity) verse *1/T*, the trap depth was estimated from the slope of the fitted dashed straight line.

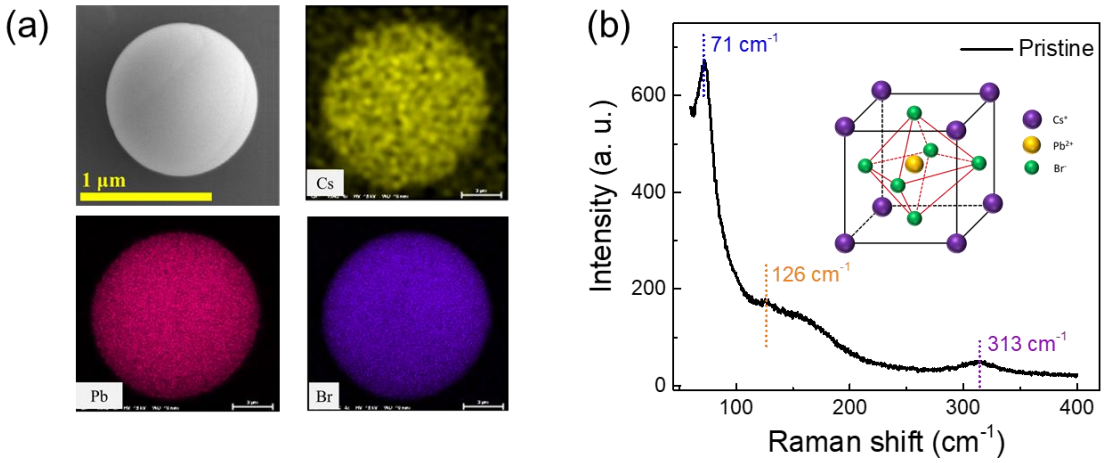

Figure S2 (a) EDS mapping of Cs, Pb, and Br for a $CsPbBr_3$ microsphere. (b) Raman spectrum of pristine $CsPbBr_3$ microspheres. The inset shows the crystal structure of $CsPbBr_3$.

The elemental mapping of Cs, Pb, and Br for a typical $CsPbBr_3$ microsphere based on energy dispersive spectrocopy (EDS) is presented in Figure S2 a. It indicates uniform spatial distributions for each element. In order to characterize the local atomic environment and bonding configuration of $CsPbBr_3$ microspheres, we also examined the Raman spectrum of $CsPbBr_3$ microspheres, as shown in the Figure S2 b. The three Raman modes with small wave numbers revealed in the Raman spectrum (a strong mode at 71 cm^{-1} and two weak modes at 126 and 313 cm^{-1}) are assigned to the vibrational modes of the $CsPbBr_3$ sublattice [3].

References:

[1] Li S, Yuan M, Zhuang W, *et al*. Optically-controlled quantum size effect in a hybrid nanocavity composed of a perovskite nanoparticle and a thin gold film. Laser Photonics Rev, 2021, 15: 2000480.

[2] Van den Eeckhout K, Bos A J J, Poelman D, *et al*. Revealing trap depth distributions in persistent phosphors. Phys Rev B, 2013, 87: 045126.

[3] Liu M, Zhao J, Luo Z, *et al*. Unveiling solvent-related effect on phase transformations in CsBr–$PbBr_2$ system: coordination and ratio of precursors. Chem Mater, 2018, 30: 5846-5852.